Journal of Power Sources 195 (2010) 263–270

Contents lists available at ScienceDirect

Journal of Power Sources

journal homepage: www.elsevier.com/locate/jpowsour

Preparation and properties of functionalized multiwalled carbon nanotubes/polypropylene nanocomposite bipolar plates for polymer electrolyte membrane fuel cells

Shu-Hang Liao[a], Cheng-Chih Weng[a], Chuan-Yu Yen[a], Min-Chien Hsiao[a], Chen-Chi M. Ma[a,*], Ming-Chi Tsai[b], Ay Su[c], Ming-Yu Yen[a], Yu-Feng Lin[d], Po-Lan Liu[a]

[a] Department of Chemical Engineering, National Tsing Hua University, Hsin-Chu 30043, Taiwan, ROC
[b] Department of Engineering and System Science, National Tsing Hua University, Hsin-Chu 30043, Taiwan, ROC
[c] Fuel Cell Center, Yuan Ze University, Tao-Yuan 32003, Taiwan, ROC
[d] Plastics Industry Development Center, Tai-Chung 40768, Taiwan, ROC

ARTICLE INFO

Article history:
Received 14 May 2009
Received in revised form 18 June 2009
Accepted 18 June 2009
Available online 26 June 2009

Keywords:
Fuel cell
Bipolar plate
Nanocomposite
Functionalized carbon nanotube
Polypropylene

ABSTRACT

Multiwalled carbon nanotubes (MWCNTs) are covalently modified with different molecular weights 400 and 2000 poly(oxyalkylene)-amine bearing the diglycidyl ether of bisphenol A (DGEBA) epoxy (POA400-DGEBA and POA2000-DGEBA) oligomers. The oxidized MWCNTs (MWCNTs-COOH) are converted to the acid chloride-functionalized MWCNTs, followed by the reaction with POA-DGEBAs to prepare the MWCNTs/POA400-DGEBA and MWCNTs/POA2000-DGEBA. FTIR, thermogravimetric analysis (TGA) and high resolution X-ray photoelectron spectra (XPS) reveal that the POA-DGEBAs are covalently attached to the surface of MWCNTs. The morphology of MWCNTs/POA-DGEBA is observed by TEM. The POA400-DGEBA coated on the MWCNTs is thicker and more uniform. However, the coating of POA2000-DGEBA on the MWCNTs shows a worm-like bulk substance and the MWCNT surface is bare. In addition, the flexural strength and the bulk electrical conductivity of the MWCNTs/polypropylene nanocomposite bipolar plates are measured 59% and 505% higher than those of the original composite bipolar plates by adding 8 phr of MWCNTs/POA400-DGEBA. The maximum current density and power density of the single cell test for the nanocomposite bipolar plate with 4 phr MWCNTs/POA400-DGEBA are 1.32 A cm^{-2} and 0.533 W cm^{-2}, respectively. The overall performance confirms the functionalized MWCNTs/polypropylene nanocomposite bipolar plates prepared in this study are suitable for PEMFC application.

1. Introduction

Recently, polymer electrolyte membrane fuel cell (PEMFC) has received intensive researches from both alternative energy and environmental consideration owing to their attractive features of high power density, low operating temperature and converting fuel to water as the only by-product [1–4]. The PEMFCs exhibit the most promising alternative source of electrical power for a variety of portable electronic devices, stationary and vehicle applications [5–7]. To generate useful currents and voltages, individual single fuel cells are connected in series to form stacks of cells. The key components of a PEMFC are the polymer electrolyte, catalyst layer, gas diffusion layer and bipolar plates. Among these components, bipolar plates provide the following main functions within the fuel cell stack [8]: provide a distribution of fuel gases within the cell, promote water management over the whole cell and exhibit excellent electrical conductivity as a current collector and provide adequate mechanical strength to resist the clamping force while the stack was assembled. Traditionally, the most used material for bipolar plate is prepared by machining graphite plate because it provides excellent corrosion resistance, low bulk density and high electrical conductivity [9–11]. However, the main difficulty in using graphite to produce bipolar plate is the time consuming and costly step of machining flow channels in the surfaces [12]. Nowadays, commercial manufactures of fuel cells are associated with major problems of high fabrication cost and insufficient reliability of fuel cells. Especially for bipolar plate (which accounts for nearly 38% in a fuel cell stack cost) [13], it is one of the most costly components in PEMFCs. Hence, the investigation on suitable materials for bipolar plates on the applications in fuel cells has become a critical research issue.

* Corresponding author at: Department of Chemical Engineering, National Tsing Hua University, 101, Section 2, Kuang Fu Road, Hsin-Chu 30043, Taiwan, ROC. Tel.: +886 3571 3058; fax: +886 3571 5408.
E-mail addresses: ccma@che.nthu.edu.tw, d937603@oz.nthu.edu.tw, d9532814@oz.nthu.edu.tw (C.-C.M. Ma).

0378-7753/$ – see front matter © 2009 Published by Elsevier B.V.
doi:10.1016/j.jpowsour.2009.06.064

In the attempt to develop an alternative material, graphite-based polymer composite bipolar plates have been considered as the substitute for the conventional graphite plates. They exhibit lower cost, higher flexibility, lighter weight and easier manufacturing, the gas flow channels can be molded directly into the plate, eliminating the requirement for a costly machining step [14]. However, the main problem of the polymer composite bipolar plate is the low electrical conductivity. Therefore, in the recent researches, graphite-based polymer composite bipolar plates have been fabricated from the combination of high concentration of graphites and additional conductive fillers to improve electrical conductivity [15–18]. Unfortunately, high carbon loading causes a substantial reduction in strength and ductility of composite bipolar plate, resulting in the difficulty of making thin plates required for high stack power densities [7,19,20]. Therefore, the reinforced fillers used commonly including carbon nanotube, carbon fiber, and carbon black which have been incorporated into the composites to enhance overall performance of composite bipolar plates by conventional polymer processing technique [18,21]. Among various reinforcements introduced into the polymer composites, carbon nanotubes (CNTs) including single walled carbon nanotubes (SWCNTs) and multi-walled carbon nanotubes (MWCNTs) possess outstanding mechanical and electrical properties that have been attracted for high-performance and multifunctional polymer composite applications [22–27]. Owing to their high flexibility, CNTs have remarkable advantage over conventional carbon fibers in processing of composites [28], in contrast to brittle carbon fibers, CNTs usually bend without failure [29]. However, there are associated with two critical issues when CNTs were used as reinforcements in polymer composites [30–32]. The major two problems including the CNTs may aggregate into bundles and only weak interfacial bonding existed between CNTs and polymer matrix limits the improvement on the electrical or mechanical properties of composites by CNTs [33]. To overcome these difficulties, this is necessary for generating strong interfacial force between fillers and the polymer. Consequently, the efficiency of the load transfer from polymer matrix to CNTs might be higher. Therefore, a better approach reported so far is the surface functionalizations of CNTs [33–38]. These functionalizations of CNTs could contribute to enhance the interaction between CNTs and the matrix, so as to provide efficient interfacial stress transfer from the polymer to CNTs. Generally, covalent functionalizations will introduce defects on the CNT surface, disrupting the extent of conjugation and adversely impacting charge carrier mobility in CNTs [39,40]. However, MWCNTs are less prone to bundle than SWCNTs and because it is possible to functionalize the surface layers only, and thus, the conductivity will not be reduced significantly [41].

In our previous study, we have found that polypropylene (PP) with lower degree of crystallinity possessed better dispersion of MWCNTs due to much more non-crystalline regions which may promote the dispersion of MWCNTs uniformly without aggregation in the PP/MWCNTs nanocomposite [7]. Apart from achieving homogeneous CNT dispersion in nanocomposites and preventing aggregation of CNTs due to Van der Waals attraction forces, the main challenge here is to enhance the interfacial compatibility between CNTs and nonpolar PP matrix. In this paper, the synthesis and characterization of two series of functionalized MWCNTs grafted on different lengths of polar polymer chain are reported. Meanwhile, functionalized MWCNTs/PP nanocomposite bipolar plates for use in fuel cells were developed by melt blending process. Furthermore, the effects of functionalized MWCNTs incorporated with PP on electrical, mechanical, thermal properties as well as their sin-

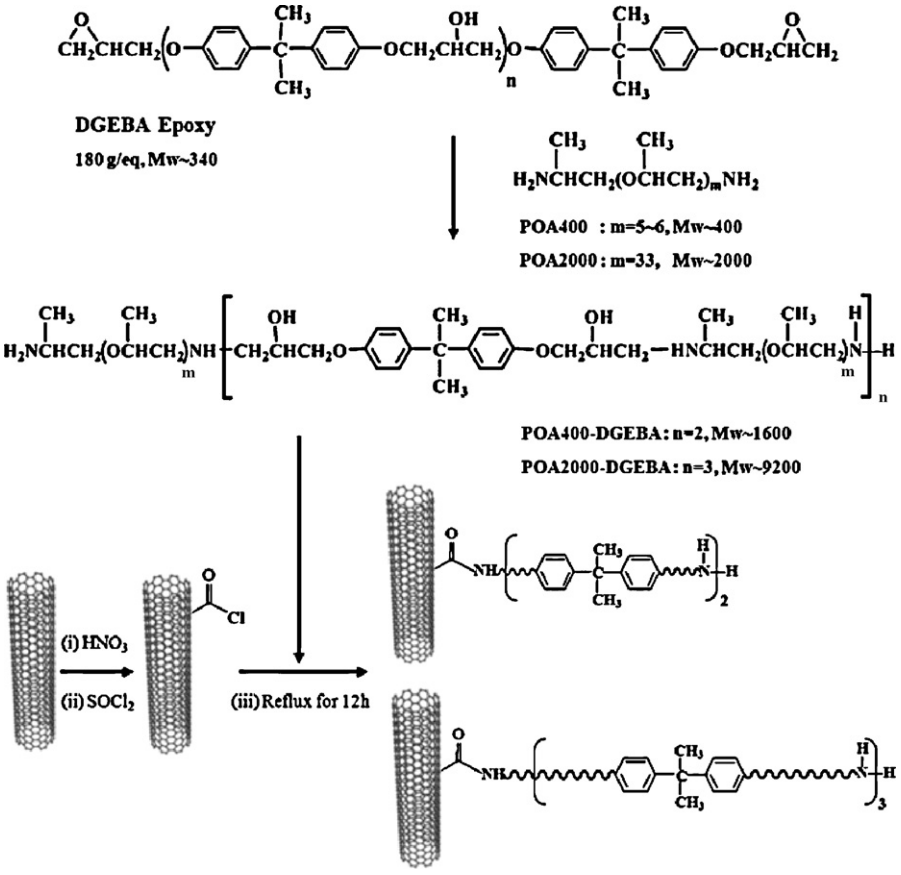

Scheme 1. Overall procedure for fabrication of MWCNTs/POA400-DGEBA and MWCNTs/POA2000-DGEBA.

gle cell performance of nanocomposite bipolar plates were also investigated.

2. Experimental

2.1. Materials

The commercial grade polypropylene (PP, was assigned as 4204 with melt flow indices (MFI) of 1.9 g/10 min) used as the polymer matrix which were supplied from the Yung Chia Chemical Ind., Co., Ltd., Taiwan. MWCNTs were received from the CNT Co., Ltd., Korea (MWCNT, trade name: $C_{tube\ 100}$, purity: 95%) with the length of 1–25 μm and average 10–50 nm in diameter. Poly(oxyalkylene)-amines (POA) were purchased from the Huntsman Chemical Co., Philadelphia, Pennsylvania, U.S.A., include poly(oxypropylene) (POP)-backboned diamines with the molecular weight M_w 400 and 2000 g mol^{-1}. Graphite powder was provided by the Great Carbon Co. Ltd., Taiwan, which has a density of 1.88 g cm^{-3} and the particle size is less than 1000 μm. The diglycidyl ether of bisphenol A (DGEBA) epoxy used in this work was supplied by the Nan Ya Plastics Co. Ltd., Taiwan, with an epoxide equivalent weight of 180 g equiv.$^{-1}$.

2.2. Preparation of MWCNTs/POA400-DGEBA and MWCNTs/POA2000-DGEBA

Scheme 1 depicts an overview of covalent grafting procedure. The preparation of various molecular weights M_w 400 and 2000 g mol^{-1} POA reacting with DGEBA (abbreviated as POA400-DGEBA and POA2000-DGEBA) was carried out in a glass reactor equipped with a stirrer. The designated amount of DGEBA (50 g, 147 mmol) was added slowly to a reactor charged with POA400 (88.2 g, 220 mmol) and POA2000 (392 g, 196 mmol), respectively, and then stirred mechanically at 25 °C for 24 h. In order to prepare MWCNTs/POA400-DGEBA and MWCNTs/POA2000-DGEBA, the oxidized MWCNTs (MWCNTs-COOH) were first achieved according to the HNO_3 washing procedure; 8 g of pristine MWCNTs were boiled in 400 ml of concentrated HNO_3 for 40 min. Then, MWCNTs-COOH were filtered, washed with 600 ml distilled water for several times to remove acid, and dried at 105 °C in an oven. During the second step, MWCNTs-COOH was converted to acid chloride-functionalized MWCNTs by refluxing in thionyl chloride for 72 h. In order to prevent excessive crosslinking of functionalized MWCNTs, a large excess POA400-DGEBA/POA2000-DGEBA was dissolved in pyridine and reacted at 70 °C for 12 h. After the amidization reaction, the mixture was separated by filtration through 0.2 μm polytetrafluoroethylene (PTFE) membrane and thoroughly washed with anhydrous THF several times to remove the residual POA400-DGEBA/POA2000-DGEBA, and then dried in a vacuum oven at 80 °C overnight to remove the solvent. Through this method, the functionalized MWCNTs (MWCNTs/POA400-DGEBA and MWCNTs/POA2000-DGEBA) could be obtained.

2.3. Preparation of MWCNTs/PP nanocomposite bipolar plates

Various MWCNTs, graphite powders and PP were melt-mixed by means of a Brabender, and then the molten compounds were obtained in the mixer. The mixing time was set at 180 °C for 10 min, and the rotational speed was 50 rpm. Then, the molten compounds were pulverized to form a powder. The powder was compression molded by a hydraulic press at a pressure of 70 kg cm^{-2} and 170 °C for 15 min. The dimensions of bipolar plate are 30 mm × 30 mm, 1.2 mm thick. The flow field pattern is serpentine and the dimensions of the channel depth and width are 1 mm × 1 mm.

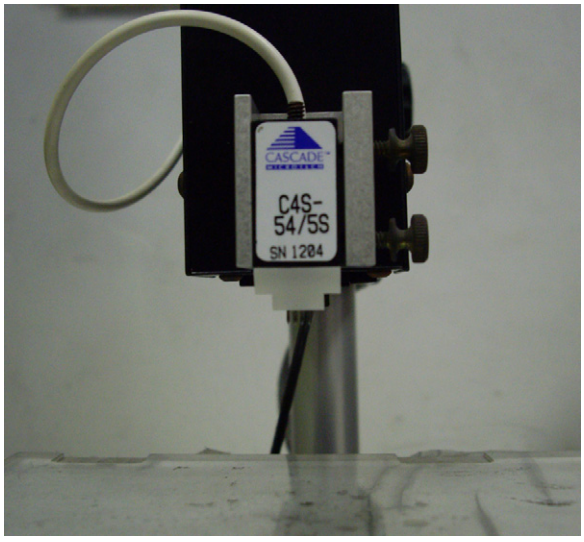

Scheme 2. Four-point probe detector.

2.4. Characterization and instruments

Gel permeation chromatography (GPC) was performed on a Waters series 510 HPLC with two PL gel 5 μm mixed columns in series. The chromatography was calibrated with polymer standards. Each sample was dissolved in tetrahydrofuran and measured with a flow rate of 0.9 ml min^{-1}. The chromatography was equipped with Waters series 410 Differential Refractometer and a TESTHIGH model 500 UV/vis Detector. Transmission electron microscope (TEM) analysis was conducted on a JEOL JEM-2100 electron microscope at 120 kV, and the samples for TEM measurements were prepared by one drop casting on carbon-coated copper grids followed by solvent evaporation in air at room temperature. Thermogravimetric analysis (TGA) was conducted utilizing a DuPont-TGA951 with a heating rate of 10 °C min^{-1} under N_2 atmosphere. FTIR spectra of the composite membranes were recorded between 1400 and 500 cm^{-1}, on a Nicolet Avatar 320 FTIR spectrometer (USA). The polymer solutions were casted onto the KBr pellet, and then dried about 5 min to evaporate the solvent. A minimum of 32 scans was signal-averaged with a resolution of 1 cm^{-1} at the 1400–500 cm^{-1} range. X-ray photoelectron spectra (XPS) measurements were performed using a VG Scientific ESCALAB 220 iXL spectrometer equipped with a hemispherical electron analyzer and an Mg Kα ($h\upsilon$ = 1487.7 eV) X-ray source. A small spot lens system allowed the analysis of a sample that was less than 1 mm^2 in area. The electrical resistivity (conductivity) of composite bipolar plate was detected using a four-point probe detector (C4S-54/5S, Cascade Microtech, Beaverton, Oregon, U.S.A.), as shown in Scheme 2. The flexural strength of composite bipolar plates with the dimensions of 60.0 mm × 13.0 mm × 3.0 mm ($L \times W \times T$) was measured by an Instron Model 4468 universal tester according to ASTM D-790 method (see Scheme 3). A single fuel cell was constructed from the prepared MEA with a platinum loading of 0.4 mg cm^{-2} for the anode and cathode, Teflon gasket, and the prepared nanocomposite bipolar plate on both sides of the MEA. The thickness of the nanocomposite bipolar plate was 1.2 mm. The single fuel cell was operated at 60 °C and 1 atm. Hydrogen and oxygen gases were fed to the anode and cathode, respectively, after passing through a bubble humidifier, and the flow rate ratio of the fuel and the oxidant was 1/1 (l min^{-1}). The performance of the single fuel cell was evaluated by measuring the *I–V* characteristics using an electronic load facility (Agilent, N3301A).

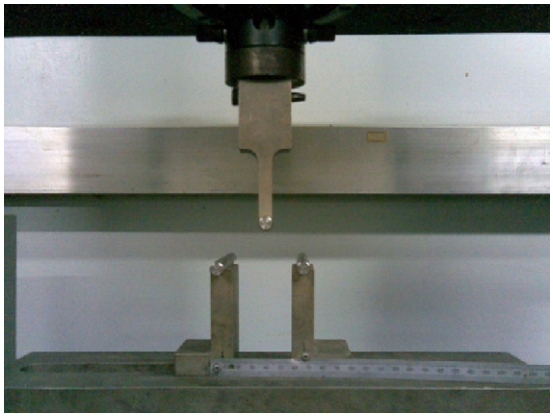

Scheme 3. The set-up of flexural strength of composite bipolar plates.

Table 1
Molecular characteristic of POA400-DGEBA and POA2000-DGEBA.

Type of oligomer	M_w (g mol^{-1})	M_n (g mol^{-1})	PDI (M_w/M_n)	Repeat unit
POA400-DGEBA	1623	697	2.3	2
POA2000-DGEBA	9231	5868	1.6	3

3. Results and discussion

3.1. Synthesis and characterizations of POA400-DGEBA and POA2000-DGEBA oligomers

Number-average (M_n) and weight-average (M_w) molecular weights, as well as polydispersity indices (PDIs, M_w/M_n), were determined for the POA400-DGEBA and POA2000-DGEBA oligomers synthesized by POA and DGEBA epoxy (Scheme 1). The molecular parameters of the resulting POA400-DGEBA and POA2000-DGEBA are summarized in Table 1. The POA400-DGEBA and POA2000-DGEBA exhibited the M_w of 1623 and 9231 with polydispersity indices (PDIs) of 2.3 and 1.6, and the calculated repeat units were 2 and 3, respectively.

3.2. Characterizations of functionalized MWCNTs (MWCNTs/POA400-DGEBA and MWCNTs/POA2000-DGEBA)

3.2.1. The morphological analysis

Fig. 1 illustrates the TEM images of the morphology and tubular structure of the pristine and functionalized MWCNTs, MWCNTs/POA400-DGEBA and MWCNTs/POA2000-DGEBA. In the TEM images of the pristine MWCNTs (Fig. 1a), the individual nanotubes were obviously a typical tangled structure and crowded bundles. At high magnification (Fig. 1b), the MWCNT wall is relatively smooth and clean. In contrast to pristine MWCNTs, MWCNTs/POA400-DGEBA and MWCNTs/POA2000-DGEBA, an organic film coating on the exterior walls of the MWCNTs was visibly observed, which cause a remarkable increase in the diameter of MWCNTs, as shown in Fig. 1c and e. For MWCNTs/POA2000-DGEBA, MWCNTs were bounded together at the intersection points. This is due to the longer polymer chains attached onto the MWCNTs probably form physical entanglements [42]. The fine nanostructures of the MWCNTs/POA-DGEBA were further investigated at high magnification (Fig. 1d and f). In the case of MWCNTs/POA400-DGEBA, the POA400-DGEBA coated on the MWCNTs was thicker and more uniform. The measured thickness of POA400-POAMA coated is varied from ~5 to 10 nm. However, the coating of POA2000-DGEBA on the MWCNTs showed a worm-like bulk substance and the MWCNT surface was bare. This is similar to the experimental observations reported by Chen et al., where the molecular weight of grafting polymers displayed a significant impact on the morphology of MWCNTs [43]. The longer POA2000-DGEBA polymer chain tends to adopt a more random coil structure.

3.2.2. Thermal stability

The contents of functionalized MWCNTs were confirmed by TGA as shown in Fig. 2. For pristine MWCNTs, there is almost no weight loss below 500°C, however, the onset of weight loss significantly occurs at a higher temperature than 500 °C, due to the thermal decomposition of the disordered carbon [44]. The organic substances of functionalized MWCNTs were degraded in the temperature range from 150 to 500 °C [45–48]. Comparing with the weight loss of pristine MWCNTs at 500 °C, the weight loss of approximately 17.1% and 27.8% was detected for MWCNTs/POA400-DGEBA and MWCNTs/POA2000-DGEBA, respectively, which may be attributed to the decomposition of

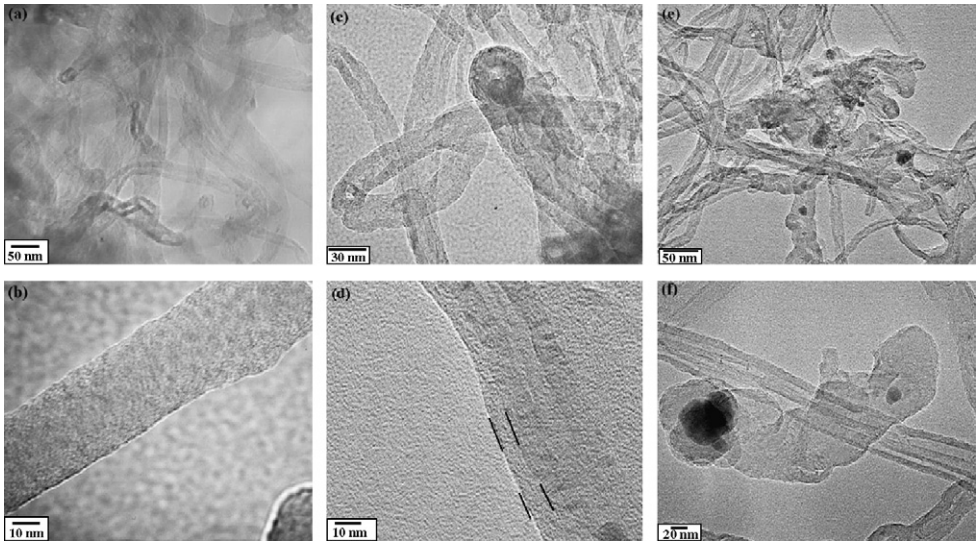

Fig. 1. TEM images of the (a and b) pristine MWCNTs, (c and d) MWCNTs/POA400-DGEBA, and (e and f) MWCNTs/POA2000-DGEBA.

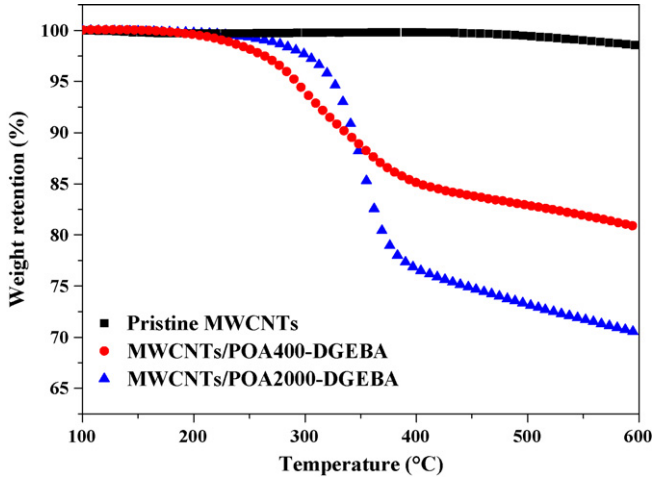

Fig. 2. TGA curves of the pristine MWCNTs, MWCNTs/POA400-DGEBA and MWCNTs/POA2000-DGEBA.

surface-grafted POA-DGEBA. The longer chain length of POA2000-DGEBA may cause that MWCNTs/POA2000-DGEBA possessed higher grafting weight yield than that of MWCNTs/POA400-DGEBA. Furthermore, the values of mol% of the POA400-DGEBA and POA2000-DGEBA moieties with respect to carbon atoms in MWCNTs ($[POA400\text{-}DGEBA]_{MWCNTs}$ = 0.29 mol% and $[POA2000\text{-}DGEBA]_{MWCNTs}$ = 0.05 mol%, respectively) were calculated by using weight percent and molecular weight of the POA400-DGEBA and POA2000-DGEBA fragment, respectively [49]. It was noticeable that the grafting density of POA-DGEBA on the MWCNTs follows the order of MWCNTs/POA400-DGEBA (0.29 mol%) > MWCNTs/POA2000-DGEBA (0.05 mol%). Apparently, the decreased grafting density was believed to be due to the increased steric hindrance effect for larger polymer molecules, i.e. M_w of POA2000-DGEBA > POA4000-DGEBA [42].

3.2.3. The surface characteristic of functional MWCNTs

The composition of the MWCNTs/POA-DGEBA was confirmed by FTIR. Fig. 3 shows the FTIR spectra of the pristine MWCNTs as well as the MWCNTs/POA400-DGEBA. The FTIR spectrum of pristine MWCNTs (Fig. 3a) displayed the peak of C=C double-bond stretching at 1635 cm^{-1} [50]. In the case of MWCNTs/POA400-DGEBA, as shown in Fig. 3b, the characteristic peak of C—O—C group on the POA400-DGEBA was strongly observed at 1105 cm^{-1} [50,51]. Moreover, the

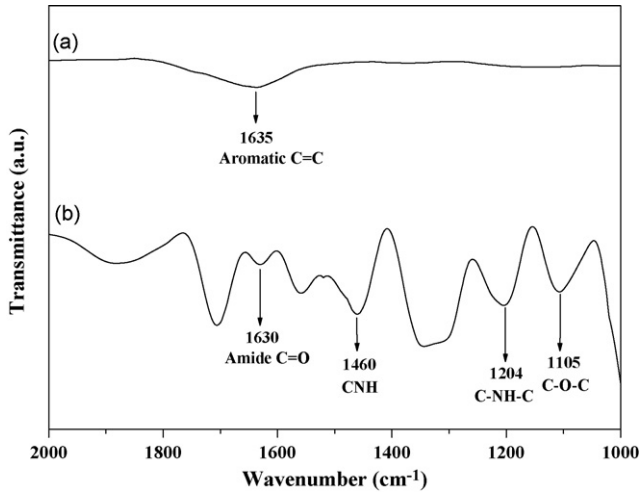

Fig. 3. FTIR spectra of (a) pristine MWCNTs and (b) MWCNTs/POA400-DGEBA.

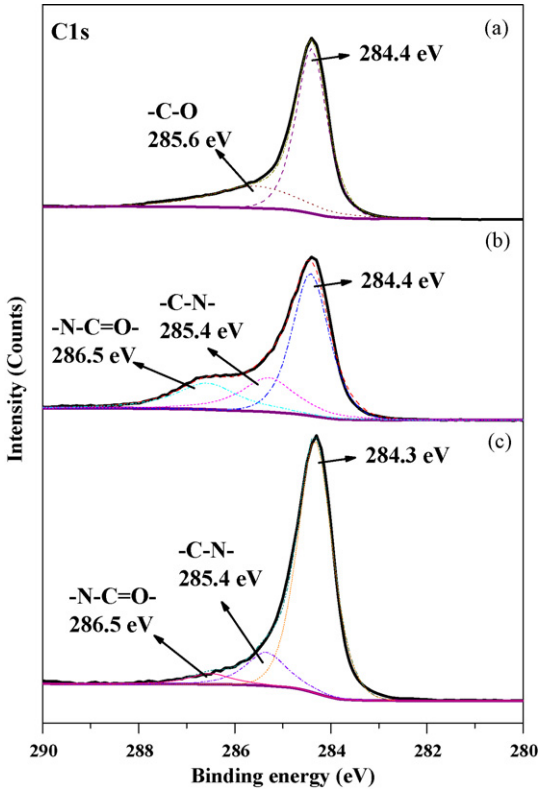

Fig. 4. X-ray photoelectron spectroscopies of pristine and chemically modified MWCNTs: C1s spectrums of (a) pristine MWCNTs, (b) MWCNTs/POA400-DGEBA and (c) MWCNTs/POA2000-DGEBA.

peak of the secondary amine (C—NH—C) appears significantly at 1204 cm^{-1}, implying the POA400-DGEBA have been effectively synthesized via the reaction of DGEBA epoxy and POA400 [50,51]. As expected, the peak observed at 1460 cm^{-1} corresponds to the CNH stretching and the peak at 1630 cm^{-1} was detected for the stretching vibration of the C=O group, respectively, due to the formation of amide linkages [52,53]. These results confirmed that POA400-DGEBA had been successfully coated on the MWCNTs.

This work also conducts qualitative analysis of XPS to elucidate the composition of the surface of functionalized MWCNTs. The C1s core level spectra of pristine and functionalized MWCNTs are presented in Fig. 4. The main sp^2 C=C, the sp^3 C—C peaks of MWCNTs appeared at 284.3–285.1 eV, additional peaks were also appeared at higher binding energies for functionalized MWCNTs indicating the presence of carbon atoms bonded to other functional groups. The binding energy peak for the pristine MWCNTs at 285.6 eV is attributed to atmospheric oxidation or residual oxides resulting from the MWCNT purification process (Fig. 4a) [14]. Besides the main C1s peaks, the resulting C1s spectrum of functionalized MWCNTs (Fig. 4b and c) could be fitted to the additional two different types of molecular structures including —C—NH_2 (285.4 eV) and —N—C=O (286.5 eV) structures, respectively [14,54,55]. Thus, the phenomenon observed in the C1s spectrum confirmed the formation of an amide linkage on the carbon nanotubes. Therefore, the XPS results further confirm that POA400-DGEBA and POA2000-DGEBA were covalently grafted onto the MWCNT surface. The shoulder peak MWCNTs/POA400-DGEBA appeared more significantly than that of MWCNTs/POA2000-DGEBA at a high binding region since the grafting density of POA400-DGEBA was much higher than that of POA2000-DGEBA on the surface of MWCNTs. This result implied that the POA400-DGEBA reacting with acid chloride-functionalized MWCNTs was more effective than does the POA2000-DGEBA. In summary, all the characteristic results

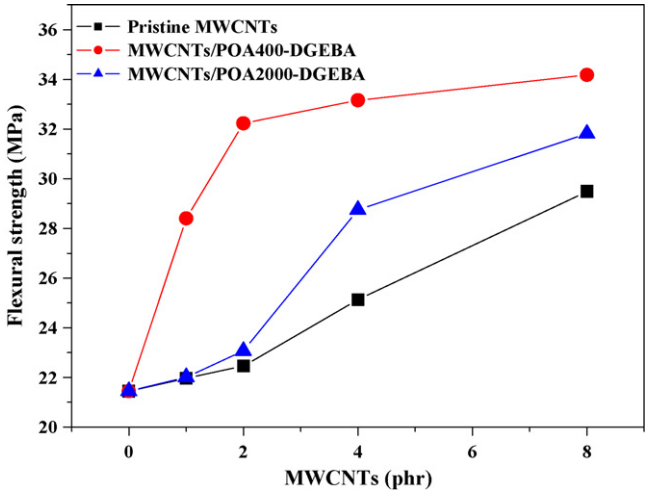

Fig. 5. The flexural strengths of the PP nanocomposite bipolar plates with 80 wt% graphite and various MWCNTs.

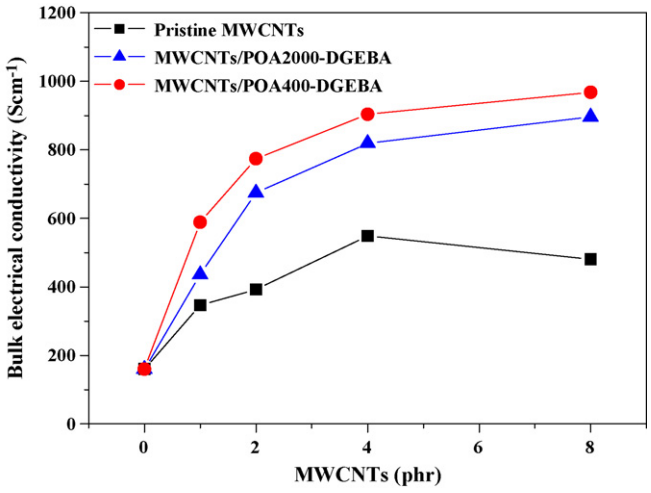

Fig. 6. The bulk electrical conductivity of the PP nanocomposite bipolar plates with 80 wt% graphite and various MWCNTs.

confirmed that the POA400-DGEBA/POA2000-DGEBA were successfully synthesized and further covalently grafted on the MWCNT surface.

3.3. Flexural strengths of MWCNTs/PP nanocomposite bipolar plates

High-performance bipolar plates should provide the required mechanical strength for PEMFC applications. However, polymer composite bipolar plates with high graphite powder loading cannot be easily formed due to the weaker adhesion between the graphite and polymer matrix. Carbon nanotubes have distinctly superior mechanical strength, which can improve the stiffness of composite materials effectively. The flexural strengths of MWCNTs/PP nanocomposite bipolar plates were measured as shown in Fig. 5. When the MWCNT content reached 8 phr, the flexural strengths of PP nanocomposite bipolar plates consisting of pristine MWCNTs, MWCNTs/POA400-DGEBA and MWCNTs/POA2000-DGEBA are 29.49, 34.18 and 31.81 MPa, respectively. All of the MWCNTs/PP nanocomposite bipolar plates are stiffer than pure composite bipolar plates without MWCNTs, which has a flexural strength of 21.44 MPa. It is believed that the increase in flexural strength is associated mainly with the rigidity, high-aspect ratio and functionalization of MWCNTs, which are critical to improve the mechanical properties of the resulting composite. The flexural strength of the nanocomposite bipolar plate with 8 phr loading of MWCNTs/POA400-DGEBA shows more than 59% improvement as compared to that of the pure composite bipolar plate without MWCNTs. This reason may result from the stronger MWCNT–polymer interaction, causing the composite bipolar plate to transfer the load from the host polymer matrix to MWCNTs more efficiently [35–38,42]. Comparing to MWCNTs/POA400-DGEBA, the serious physical polymer chain entanglements and bared surface on the MWCNTs/POA2000-DGEBA may cause worse compatibilities between MWCNTs and PP matrix (as shown in Fig. 1c). Nevertheless, the MWCNTs/POA400-DGEBA/PP nanocomposite bipolar plates with better compatibility between fillers and polymer resin show the greater enhancement of the flexural strength.

3.4. Bulk electrical conductivity of MWCNTs/PP nanocomposite bipolar plates

A number of reports indicated that the incorporation of graphite with other conductive materials, especially carbon nanotubes, have been considered as an effective method to develop higher bulk electrical conductivity of the nanocomposite bipolar plates due to 3D conductive networks [30–33]. Fig. 6 exhibits the bulk electrical conductivity of nanocomposite bipolar plates as a function of MWCNT content. Three types of MWCNTs/PP nanocomposite bipolar plates show promising bulk electrical conductivity, above the D.O.E. target value of 100 S cm^{-1}. Meanwhile, results also show that the bulk electrical conductivities of the PP nanocomposite bipolar plates increased dramatically with the increasing of MWCNT content. As the MWCNT content was 8 phr, the bulk electrical conductivities of MWCNTs/POA400-DGEBA, MWCNTs/POA2000-DGEBA, and pristine MWCNTs/PP nanocomposite bipolar plates are measured at 968, 896 and 481 S cm^{-1}, respectively. Bulk electrical conductivity increases significantly in the order of MWCNTs/POA400-DGEBA > MWCNTs/POA2000-DGEBA > pristine MWCNTs/PP nanocomposite bipolar plates, for a given MWCNT content. For pristine MWCNTs, the formation of local MWCNT aggregations tend to increase the number of filler–filler hops required to traverse a given distance, thus causing the decrease of bulk electrical conductivity at high MWCNT loading. Although, the longer chain of POA2000-DGEBA has better repulsion effect between the MWCNTs than does POA400-DGEBA, which will prevent from bundling due to Van der Waals forces between the MWCNTs. The serious physical polymer chain entanglements and more bared surfaces on the MWCNTs/POA2000-DGEBA would cause the aggregation of MWCNTs and non-uniform MWCNT dispersion in the PP matrix. Fig. 7 proposed a dispersion diagram of functionalized MWCNTs in the PP nanocomposite bipolar plate with MWCNTs/POA400-DGEBA and MWCNTs/POA2000-DGEBA, respectively. Comparing these two dispersant models of functionalized MWCNTs, it is assumed that more electrical conductive paths were formed more effectively by introducing the MWCNTs/POA400-DGEBA than does MWCNTs/POA2000-DGEBA in PP nanocomposite bipolar plates.

3.5. Single fuel cell performance of MWCNTs/PP nanocomposite bipolar plates

Figs. 8 and 9 present the *I–V* and *I–P* performance of the single cells compressively assembled with 4 phr pristine MWCNTs, MWCNTs/POA400-DGEBA, MWCNTs/POA2000-DGEBA and graphite composite bipolar plates, respectively. The open circuit voltage (OCV) of single cells is almost the same at 1.1 V as shown in Fig. 8. At first, over the middle current density region, the improved

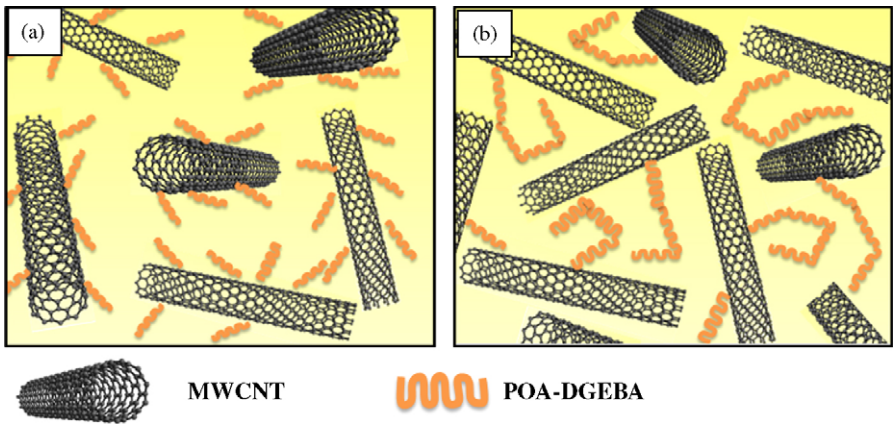

Fig. 7. The dispersion diagram of MWCNTs in the PP nanocomposite bipolar plate of (a) MWCNTs/POA400-DGEBA and (b) MWCNTs/POA2000-DGEBA systems.

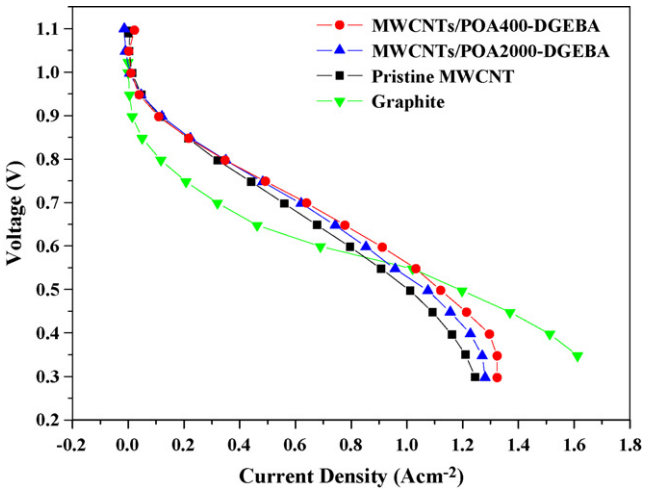

Fig. 8. *I–V* curves of the single cells assembled with graphite plates and various MWCNTs/PP nanocomposite bipolar plates.

performance could be observed. It is postulated that the flexibility of MWCNTs/PP nanocomposite bipolar plates could effectively help to reduce the interfacial contact resistance between the MEA and bipolar plates during the compressively assembling of a single cell. Therefore, the single cell using MWCNTs/PP nanocomposite bipolar plates exhibited lower ohmic resistance than using pure graphite bipolar plates, and thus leading to higher performance. The differences of *I–V* curves of the fuel cell with graphite and MWCNTs based bipolar plates are most likely caused by difference in the wetting behavior of bipolar plates in the low and high current density regions. From water contact angle data, as shown in Fig. 10, results indicated that pristine MWCNTs, MWCNTs/POA400-DGEBA and MWCNTs/POA2000-DGEBA/PP nanocomposite bipolar plates with relatively smaller water contact angles (approaching 80.5°, 81° and 82°, respectively) than that of graphite bipolar plates (approaching 87°). The hydrophilic MWCNTs based nanocomposite bipolar plates with poor water suction from the GDL may cause difficulty in water transfer, and thus, no limiting current was observed. Contrarily, the hydrophobic graphite bipolar plates could repel water from the cathode well [56]. Meanwhile, this implied that catalyst/electrode was dry at low current density, leading to larger activation losses. Moreover, Fig. 8 shows the current density of single cells increases in the order of MWCNTs/POA400-DGEBA > MWCNTs/POA2000-DGEBA > pristine MWCNTs. The maximum current densities are 1.32, 1.28, 1.08, and 1.24 A cm^{-2}, respectively. Meanwhile, the maximum power density of the single cell consisting of MWCNTs/POA400-DGEBA/PP nanocomposite bipolar plates is 0.552 W cm^{-2}, only 11% lower than that of graphite bipolar plates (0.614 W cm^{-2}) as shown in Fig. 9. Appar-

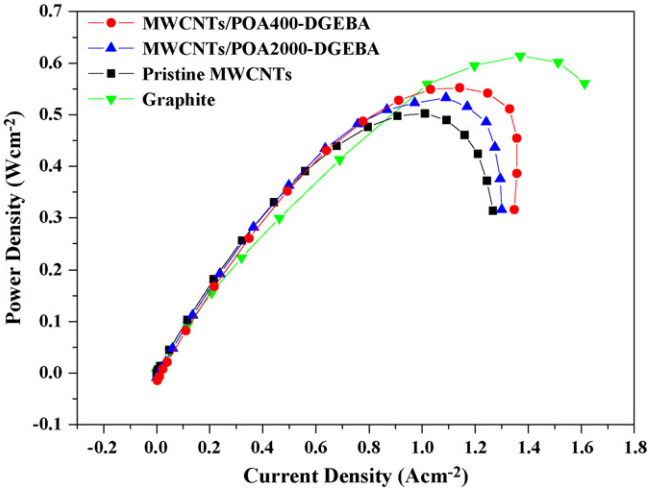

Fig. 9. *I–P* curves of the single cells assembled with graphite plates and various MWCNTs/PP nanocomposite bipolar plates.

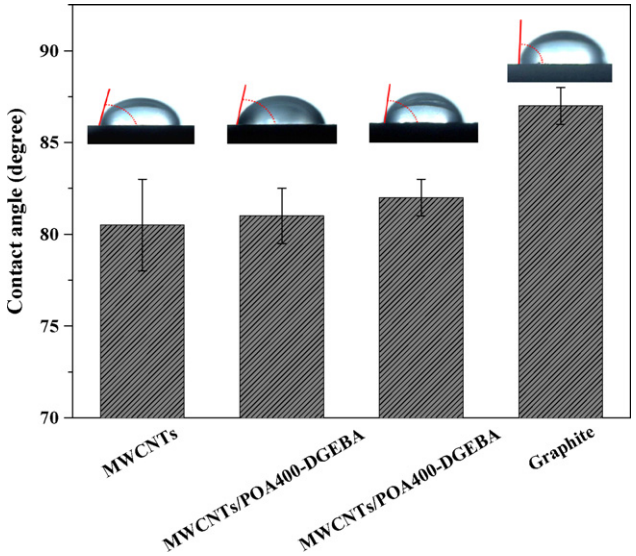

Fig. 10. Water contact angles of graphite and MWCNTs/PP nanocomposite bipolar plates.

ently, the nanocomposite bipolar plates-MWCNTs/POA400-DGEBA presented in this study provide better results than other types of MWCNTs/PP nanocomposite bipolar plates for two reasons: (1) the dispersion of MWCNTs/POA400-DGEBA is better than the dispersion associated with other MWCNTs; (2) more continuous electrical conducting paths will promote the transfer of electrons in PEMFC. All results presented in Figs. 8 and 9 demonstrate that MWCNTs/POA400-DGEBA/PP nanocomposite bipolar plates developed in this study possess comparable single cell performance to graphite bipolar plates which could be the alternative bipolar plate materials for high-cost machined graphite.

4. Conclusions

In this study, a novel PP nanocomposite bipolar plate with functionalized MWCNTs, has been prepared successfully by melt blending of PP, graphite powder and functionalized MWCNTs and then compression molding. Results reveal the PP nanocomposite bipolar plates by introducing the pristine and two functionalized MWCNTs possessed improved bulk electrical conductivity and flexural strength. Especially for MWCNTs/POA400-DGEBA system, the mechanical and electrical properties of MWCNTs/PP nanocomposite bipolar plate were increased dramatically, due to the better dispersion of MWCNTs. Consequently, higher flexural strength and superior electrical conductivity can be achieved. This phenomenon could be explained that the higher polymer chain grafting density and uniform polymer coating on the MWCNTs/POA400-DGEBA would improve the flexural strength and bulk electrical conductivity of composite bipolar plate effectively. Moreover, the MWCNTs/POA400-DGEBA/PP nanocomposite bipolar plates also exhibit lower ohmic resistance than graphite bipolar plates, and thus leading to higher fuel cell performance at the median current density region. The overall performance shows that the MWCNTs/POA400-DGEBA/PP nanocomposite bipolar plates developed in this work perform excellently for PEMFCs.

Acknowledgements

The authors are grateful to the Ministry of Economic Affairs, Taiwan, Republic of China for financial support. The support from Yuan Ze Fuel Cell Center, Taiwan, Republic of China, is also greatly appreciated.

References

[1] B.C.H. Steele, A. Heinzel, Nature 414 (2001) 345.
[2] H.C. Kuan, C.C.M. Ma, K.H. Chen, S.M. Chen, J. Power Sources 134 (2004) 7.
[3] A. Hermann, Int. J. Hydrogen Energy 30 (2005) 1297.
[4] A. Muller, P. Kauranen, A.V. Ganski, B. Hell, J. Power Sources 154 (2006) 467.
[5] S.H. Liao, C.H. Hung, C.C.M. Ma, C.Y. Yen, Y.F. Lin, C.C. Weng, J. Power Sources 176 (2008) 175.
[6] B.D. Cunningham, J. Huang, D.G. Baird, J. Power Sources 165 (2007) 764.
[7] S.H. Liao, C.Y. Yen, C.C. Weng, Y.F. Lin, C.C.M. Ma, C.H. Yang, M.C. Tsai, M.Y. Yen, M.C. Hsiao, S.J. Lee, X.F. Xie, Y.H. Hsiao, J. Power Sources 185 (2008) 1225.
[8] L. Du, S.C. Jana, J. Power Sources 172 (2007) 734.
[9] G.O. Mepsed, J.M. Moore, Handbook of Fuel Cells—Fundamentals, Technology and Application, John Wiley and Sons, Ltd., New York, 2003, pp. 286–293.
[10] A.A. Kulikovsky, J. Power Sources 160 (2006) 431.
[11] T. Yang, P. Shi, J. Power Sources 175 (2008) 390.
[12] K. RoBberg, V. Trapp, Handbook of Fuel Cells—Fundamentals, Technology and Applications, John Wiley & Sons, Ltd., New York, 2003, pp. 308–314.
[13] S.R. Dhakate, R.B. Mathur, B.K. Kakati, T.L. Dhami, Int. J. Hydrogen Energy 32 (2007) 4537.
[14] S.H. Liao, C.Y. Yen, C.H. Hung, C.C. Weng, M.C. Tsai, Y.F. Lin, C.C.M. Ma, C. Pan, A. Su, J. Mater. Chem. 18 (2008) 3993.
[15] J.K. Kuo, C.K. Chen, J. Power Sources 162 (2006) 207.
[16] I.E. Paulauskas, M.P. Brady, H.M. Meyer III, R.A. Buchanan, L.R. Walker, Corros. Sci. 48 (2006) 3157.
[17] B.D. Cunningham, D.G. Baird, J. Power Sources 168 (2007) 418.
[18] C.Y. Yen, S.H. Liao, Y.F. Lin, C.H. Hung, Y.Y. Lin, C.C.M. Ma, J. Power Sources 162 (2006) 309.
[19] M. Wu, S.L. Leon, J. Power Sources 136 (2004) 37.
[20] L.D. Andrew, J. Power Sources 156 (2006) 128.
[21] J. Scholta, B. Rohland, V. Trapp, U. Focken, J. Power Sources 84 (1999) 231.
[22] L. Sun, G.L. Warren, J.Y. O'Reilly, W.N. Everett, S.M. Lee, D. Davis, D. Lagoudas, H.-J. Sue, Carbon 46 (2008) 320.
[23] S. Wang, R. Liang, B. Wang, C. Zhang, Chem. Phys. Lett. 457 (2008) 371.
[24] G.L. Hwang, Y.T. Shieh, K.C. Hwang, Adv. Funct. Mater. 14 (2004) 487.
[25] R. Blake, J.N. Coleman, M.T. Byrne, J.E. McCarthy, T.S. Perova, W.J. Blau, A. Fonseca, J.B. Nagy, Y.K. Gun'ko, J. Mater. Chem. 16 (2006) 4206.
[26] H. Xia, M. Song, J. Mater. Chem. 16 (2006) 1843.
[27] J. Zhu, H. Peng, F. Rodriguez, J.L. Margrave, V.N. Khabashesku, A.M. Imam, K. Lozano, E.V. Barrera, Adv. Funct. Mater. 14 (2004) 643.
[28] P.M. Ajayan, Chem. Rev. 99 (1999) 1796.
[29] P.M. Ajayan, J.M. Tour, Nature 447 (2007) 1067.
[30] D.M. Delozier, K.A. Watson, J.G. Smith Jr., T.C. Clancy, J.W. Connell, Macromolecules 39 (2006) 1731.
[31] Y. Yang, X. Xie, J. Wu, Z. Yang, X. Wang, Y.W. Mai, Macromol. Rapid Commun. 27 (2006) 1695.
[32] O. Lourie, H.D. Wagner, Appl. Phys. Lett. 73 (1998) 3527.
[33] D.H. Xu, Z.G. Wang, Macromolecules 41 (2008) 815.
[34] D.H. Xu, Z.G. Wang, Polymer 49 (2008) 330.
[35] A.A. Koval'chuk, A.N. Shchegolikhin, V.G. Shevchenko, P.M. Nedorezova, A.N. Klyamkina, A.M. Aladyshev, Macromolecules 41 (2008) 3149.
[36] A.A. Koval'chuk, V.G. Shevchenko, A.N. Shchegolikhin, P.M. Nedorezova, A.N. Klyamkina, A.M. Aladyshev, Macromolecules 41 (2008) 7536.
[37] D. McIntosh, V.N. Khabashesku, E.V. Barrera, Chem. Mater. 18 (2006) 4561.
[38] D. McIntosh, V.N. Khabashesku, E.V. Barrera, J. Phys. Chem. C 111 (2007) 1592.
[39] J. Zhao, H. Park, J. Han, J.P. Lu, J. Phys. Chem. B 108 (2004) 4227.
[40] E. Bekyarova, M.E. Itkis, N. Cabrera, B. Zhao, A.P. Yu, J.B. Gao, R.C. Haddon, J. Am. Chem. Soc. 127 (2005) 5990.
[41] R.A. Hatton, A.J. Miller, S.R.P. Silva, J. Mater. Chem. 18 (2008) 1183.
[42] L. Xie, F. Xu, F. Qiu, H. Lu, Y. Yang, Macromolecules 40 (2007) 3296.
[43] G.X. Chen, H.S. Kim, B.H. Park, J.S. Yoon, J. Phys. Chem. B 109 (2005) 22237.
[44] Y.L. Hsin, K.C. Hwang, C.T. Yeh, J. Am. Chem. Soc. 129 (2007) 9999.
[45] V. Datsyuk, M. Kalyva, K. Papagelis, J. Parthenios, D. Tasis, A. Siokou, I. Kallitsis, C. Galiotis, Carbon 46 (2008) 833.
[46] A.D. Christopher, M.T. James, Nano Lett. 3 (2003) 1215.
[47] H.M. Huang, C.Y. Chang, H.C. Tsai, C.H. Hsu, R.C. Tsiang, I.C. Liu, Macromolecules 37 (2004) 283.
[48] S. Chen, W. Shen, G. Wu, D. Chen, M. Jiang, Chem. Phys. Lett. 402 (2005) 312.
[49] D. Baskaran, J.W. Mays, M.S. Bratcher, Angew. Chem. Int. Ed. 43 (2004) 2138.
[50] N.B. Colthup, L.H. Daly, S.E. Wiberley, Introduction to Infrared and Raman Spectroscopy, third edition, Academic Press Inc., 1990.
[51] S.T. Lin, K.L. Wei, T.M. Lee, K.C. Chiou, J.J. Lin, Nanotechnology 17 (2006) 3197.
[52] J. Gao, B. Zhao, M.E. Itkis, E. Bekyarova, H. Hu, V. Kranak, A. Yu, R.C. Haddon, J. Am. Chem. Soc. 128 (2006) 7492.
[53] S.A. Evenson, C.A. Fail, J.P.S. Badyal, Chem. Mater. 12 (2000) 3038.
[54] C.H. Tseng, C.C. Wang, C.Y. Chen, Chem. Mater. 19 (2007) 308.
[55] S.E. Baker, W. Cai, T.L. Lasseter, K.P. Weidkamp, R.J. Hamers, Nano Lett. 2 (2002) 1413.
[56] S. Chunhui, P. Mu, H. Zhoufa, Y. Runzhang, J. Power Sources 166 (2007) 419.